Flow over bedforms in a large sand-bed river: A field investigation

Ecoulements sur des configurations de lits sableux de grands fleuves: investigation en nature

ROBERT R. HOLMES, JR., Hydrologist, *U.S. Geological Survey Office of Surface Water, 1201 W. University Avenue, Urbana, Illinois 61801, USA. E-mail: bholmes@usgs.gov*

MARCELO H. GARCIA, (IAHR Member), Siess Professor and Director, *Ven Te Chow Hydrosystems Laboratory, University of Illinois at Urbana-Champaign, 205 N. Matthews, Urbana, Illinois, 61801, USA. E-mail: mhgarcia@uiuc.edu*

ABSTRACT

An experimental field study of flows over bedforms was conducted on the Missouri River near St. Charles, Missouri. Detailed velocity data were collected under two different flow conditions along bedforms in this sand-bed river. The large river-scale data reflect flow characteristics similar to those of laboratory-scale flows, with flow separation occurring downstream of the bedform crest and flow reattachment on the stoss side of the next downstream bedform. Wave-like responses of the flow to the bedforms were detected, with the velocity decreasing throughout the flow depth over bedform troughs, and the velocity increasing over bedform crests. Local and spatially averaged velocity distributions were logarithmic for both datasets. The reach-wise spatially averaged vertical-velocity profile from the standard velocity-defect model was evaluated. The vertically averaged mean flow velocities for the velocity-defect model were within 5% of the measured values and estimated spatially averaged point velocities were within 10% for the upper 90% of the flow depth. The velocity-defect model, neglecting the wake function, was evaluated and found to estimate the vertically averaged mean velocity within 1% of the measured values.

RÉSUMÉ

Une étude expérimentale en nature des écoulements sur des formes de lit a été conduite sur le fleuve Missouri près de St. Charles, Missouri. Des données détaillées de vitesse ont été rassemblées dans deux conditions différentes d'écoulement le long des formes du lit dans ce fleuve sableux. Les données à l'échelle des grands fleuves reflètent des caractéristiques d'écoulement semblables à celles des écoulements en laboratoire, avec la séparation d'écoulement se produisant en aval de la crête de dune et le recollement de l'écoulement sur la face de la dune suivante Des réponses de sillage de l'écoulement aux dunes ont été détectées, avec la vitesse diminuant dans tout le tirant d'eau au-dessus des creux, et la vitesse augmentant au dessus des crêtes. Les distributions des vitesses moyennes locales et spatiales étaient logarithmiques pour les deux ensembles de données. L'écart du profil des vitesses moyennes dans l'espace ramené au modèle standard de défaut de vitesse a été évalué. Les vitesses moyennes verticales ramenées à une moyenne d'écoulement pour le modèle de défaut de vitesse étaient à moins de 5% des valeurs mesurées et les vitesses moyennes dans l'espace étaient à moins de 10% pour les 90% du tirant d'eau supérieur. Le modèle de défaut de vitesse, négligeant la fonction de sillage, a été évalué pour estimer la vitesse moyenne sur la verticale à moins de 1% des valeurs mesurées.

1 Introduction

Bedforms occur on the bottom of sand-bed rivers and result in flow that is complex and dynamic. The bedforms are an obstacle to the flow and cause both wake effects in their lee and topographically induced spatial flow acceleration, which is termed wave-like effects. In a general longitudinal sense, bedforms cause a momentum defect that diffuses outward in the downstream direction. Flow separation occurs near the bedform crest, followed by a reattachment of the flow on the next downstream bedform (Fig. 1). At the reattachment point (where a definable velocity profile begins to re-develop near the bed), a new internal boundary layer begins to grow within the wake region.

Much research has been conducted pertaining to the flow hydrodynamics over bedforms found in sand-bed rivers. Most

of this work, however, has been conducted in laboratory flumes (Bennett and Best, 1995; Lyn, 1993; Nelson *et al.*, 1993), primarily because of the difficult logistics and expense of collecting and analyzing field data, particularly on large rivers of depths from approximately 3 to 15 m and mean annual discharges $\geq 500\,\text{m}^3/\text{s}$. Obviously, there are questions of scale effects when theories or algorithms derived from laboratory research are applied to large sand-bed rivers. There is a need for data on large sand-bed rivers to establish means for either enhancing present theories (based on the laboratory data) or developing entirely new theories. Consider the following expressed by ASCE (2002):

"Field studies with detailed measurements of not only dune characteristics but also flow and transport are valuable and daunting for the same reason: they indicate the complexity of the real problem, which, together with practical constraints on field measurements, make more difficult the analysis and interpretation of the data."
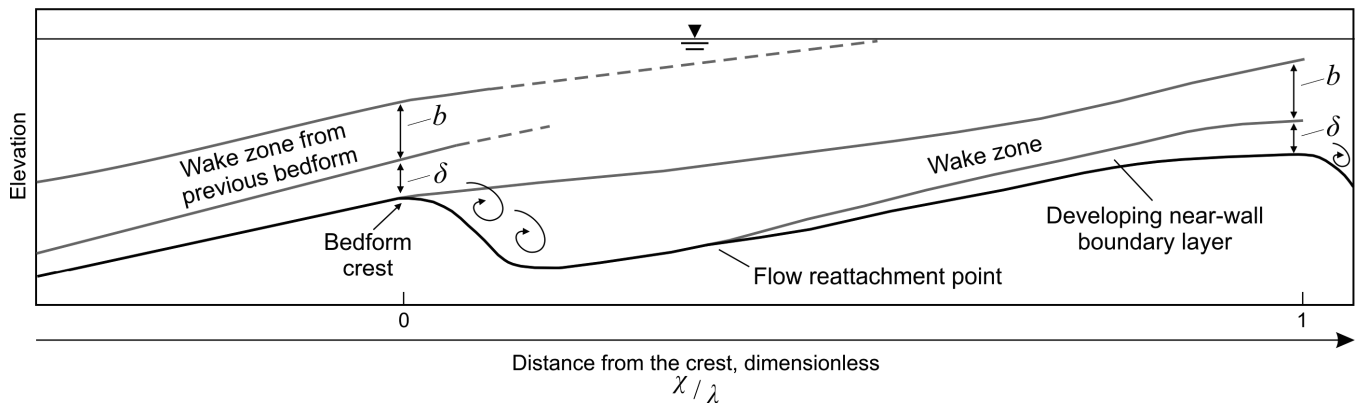
Figure 1   Flow over a bedform where δ is the developing internal boundary layer and b is the developing wake zone resulting in a momentum defect

Correct understanding and prediction of the velocity profile and associated flow resistance is necessary for flow measurement, sediment transport prediction, and model simulation of sand-bed river systems. The combination and interaction of the turbulence field and flow accelerations because of the non-uniformity of the bed are reported to affect the form drag of the bedforms (Nelson *et al.*, 1993). Consideration of the flow resistance is important for hydraulic engineers in determining the relation between discharge and stage.

Determination of the flow physics of the near-bed region is crucial for understanding the relation between bedform geometry and flow properties. The near-bed region is an area of intense turbulence generation and concurrent mean flow energy loss. Because of the difficulties of data collection at depth in large sand-bed rivers, the data are scant in the near-bed region. More detailed velocity data in the vicinity of bedforms are needed to increase the understanding of the flow field in these areas. This work presents an overview of the measurement devices, and describes the experimental setup and results of the analysis of data collected at the Missouri River at St. Charles, Missouri. Results from this study should enhance the understanding of flow over bedforms in large sand-bed rivers, particularly in the near-bed region.

2   Hydraulics of flow over bedforms

The velocity in a shear flow is non-uniform because of the presence of the boundary and the resulting resistance to flow not only along the boundary but between the fluid particles. Although it was realized as early as in the 4th Century B.C. by Aristotle that flow resistance was important to the bulk flow (Rouse and Ince, 1963), it was not until Prandtl (1904) presented his paper on the boundary-layer theory that fluid mechanics was incorporated into flow-resistance theory and enabled a characterization of the profile of the velocity distribution in the vertical (Yen, 1992). Alluvial channels add a layer of complexity to any investigation into the flow field because of the capacity of the boundary geometry to change with flow condition.

In laboratory experimental observations, it has been noted that in flow over a train of bedforms, a definitive momentum defect region is present (Nelson *et al.*, 1993; Bennett and Best, 1995). This region is associated with flow separation and wake formation

downstream of the bedform lee face, and as the wake is advected downstream, the effect of the momentum defect is diffused outward, causing the region to grow in depth. A conceptual drawing of the flow character in the presence of bedforms is given in Fig. 1. The flow separates at the crest of the bedform and reattaches at some point downstream on the next bedform, creating an adverse pressure gradient

$$\frac{1}{\mu}\frac{dp}{dx} > 0 \tag{1}$$

where p is pressure, μ dynamic viscosity, and x the streamwise coordinate. The pressure gradient induces a smaller velocity gradient and, thus, a smaller velocity near the bed given as

$$\left.\frac{\partial^2 u}{\partial z^2}\right|_{z=0} = \frac{1}{\mu}\frac{dp}{dx} > 0 \tag{2}$$

where u is the streamwise velocity and z is the vertical coordinate. From laboratory experiments of Nelson *et al.* (1993), the reduction of bed velocity in the presence of adverse pressure gradients is well demonstrated on the stoss side of the bedform.

For a shear flow over a flat-rough bed, the velocity profile has been found empirically to be acceptably approximated by Prandtl's logarithmic law of the wall equation for the entire depth of the flow (Garcia, 1999) expressed as

$$\frac{u}{u_*} = \frac{1}{\kappa}\ln z + C \tag{3}$$

where u_* is the shear velocity, κ is von Karman's constant, and C is a constant. For shear flows over a flat-rough bed, the Reynolds stresses typically decrease monotonically away from the boundary, reaching zero near the water surface in equilibrium conditions. With bedforms present, the velocity and Reynolds stress profiles have been shown experimentally to be different from those for a flat-rough bed (Bennett and Best, 1995; Nezu and Nakagawa, 1993). The velocity profiles for these experiments were logarithmic in nature; however, the slopes vary in multiple and separate distinct layers. The major separation point between the layers often corresponds to a maximum in the Reynolds stress, increasing from the boundary to the location of the maximum shear stress and then decreasing toward the water surface.

3   Review of past field experiments

As expressed earlier, there is a lack of field-scale experiments of detailed velocity measurements longitudinally over bedforms, especially for large river systems. Two notable exceptions are the field experiments of Smith and McLean (1977) and Kostaschuk and Villard (1996).

Smith and McLean (1977) conducted experiments on the Columbia River (USA) in which they collected data on velocity and sediment-concentration profiles over bedforms as well as channel bathymetry and bed-material samples for a sediment-size analysis. In these experiments, velocity was measured at four locations in the boundary layer using 0.04 m diameter mechanical current meters attached to a frame that was lowered to the near bed. Other velocity observations were made with a suspended device. The frame was moved 3 m downstream every hour. The discharge during the experiments ranged from 8000 to 17 000 m^3/s, with velocities 1 m from the bed ranging from 0.50 to 0.82 m/s. In the early experiments (1968 and 1969), the sediment was transported only as bedload, whereas during the 1971 and 1972 experiments sediment was transported as both suspended-sediment load and bedload. In the experiments with bedload only, the bedforms were shorter and steeper than for the other experiments. The elongated, more symmetrical bedforms were not sufficient to induce separated flow in the lee of the bedform. Velocity data were collected at time scales such that in examining velocity profiles, the velocity data were averaged over 30 minutes at multiple locations in the vertical and then averaged in the longitudinal direction (along the bedform). The velocity data also were normalized with the velocity measured 1 meter above the bed, as opposed to normalizing with the shear velocity, which is more typical. Depths ranged from 13.4 to 16.6 m, with bedforms ranging from 67 to 96 m in length and from 1.34 to 3.21 m in height.

Kostaschuk and Villard (1996) collected flow and sediment data over asymmetric and symmetric bedforms in the Fraser River estuary near Steveston, Canada. Data were collected between May and July 1989 at 4 to 5 verticals along the bedforms. They found no lee-side flow separation for flows over the bedforms. A Marsh McBirney™ 527 current meter and pump sampler were secured above a 70 kg lead sounding weight to collect the necessary velocity and sediment data for this study.

4   Experimental procedure

A reach of the Missouri River at St. Charles, Missouri was chosen for study because it provided (1) good logistics with a boat launch adjacent to the data-collection reach; (2) approximate equilibrium dimensions for dunes with dune height to water-depth ratios from 1/6 to 1/7; and (3) "pseudo-steady" flow conditions for duration of data collection of 10 to 15 hours. Two sets of data were collected. The first set, designated MO-1, was collected on June 19, 2002 and the second set, designated MO-2, on August 27, 2002.

In the study reach, the river is fairly straight and flows to the northeast. The study reach is 44.6 km upstream from the confluence with the Mississippi River. USGS streamflow-gaging station 06935965 is immediately adjacent to the study reach, a gaging station is maintained by the Corps of Engineers 44.6 km downstream on the Mississippi River at Alton, Ill. near the confluence of the Missouri River, and a wire-weight gage is maintained by the National Weather Service 53 km upstream at Washington, Mo. The water surface slopes for these experiments were determined by utilizing the water surface elevations at these locations. The slope in the reach upstream of St. Charles is typically higher than the reach downstream. As the reach of gages extends 97.6 km, the true slope at St. Charles will differ from the reach-averaged slope. The reach-averaged slope is reasoned to be an acceptable estimate of the water surface slope because the reach-averaged (bulk) shear stress computed from the product of the water-surface slope, flow depth, and acceleration of gravity compares well with the reach-averaged shear stress computed from the spatially averaged velocity profile.

The channel bed is composed of fairly uniform sand with $D_{50} = 0.31$ mm. The channel-top width at the study reach for bank-full flows is between 350 and 400 m at the discharges present during data-collection efforts in this study. The approximate bank-full flow depth would be around 9 m. The flows at times of data collection for this research were well within the channel banks, with average water depths for MO-1 and MO-2 of 6.4 and 5.0 m, respectively. Both banks are lined with trees and riprap.

For each dataset, the bathymetry data were collected using a boat-mounted 200 kHz Odum Hydrographic Systems Hydrotrac Digital Fathometer, with 1 cm accuracy, in concert with a Trimble AgGPS™ 124/132 differentially corrected global positioning system (DGPS), with sub-meter horizontal accuracy. The data from these instruments were synchronized and logged using Oceangraphic Systems, Inc. HYPACK™ software.

Detailed velocity data were collected from a stationary boat using a down-looking 600 kHz acoustic Doppler current profiler (ADCP) and multiple 10 MHz acoustic Doppler velocimeters (ADV). Single ping per ensemble velocity data were collected at 3 Hz using the ADCP with typical median absolute deviations (MAD) (Helsel and Hirsch, 1992) between 0.17 and 0.19 m/s. Single ping per ensemble data were collected at 25 Hz using the ADV with typical MAD values between 0.05 and 0.15 m/s depending on location in the water column, with higher MAD values for those locations near the bed. The horizontal position of each vertical was determined by DGPS. The ADCP was mounted to the side of the boat; one of the ADVs was mounted on a modified P-61 sediment sampler suspended from the boat by a cable (Fig. 2) and the other on the boat to obtain a surface velocity. The surface-velocity data from the ADV mounted to the boat was not used to determine the velocity profiles as the presence of the boat caused a decrease in the stream velocities near the surface. Attempts (with limited success) were made to collect suspended-sediment data by both a pump sampler connected to intakes on the modified P-61 sediment sampler and through the regular sampling capacity of the P-61.

To begin the collection of the detailed velocity data, two anchors were deployed from the boat upstream on each side of the
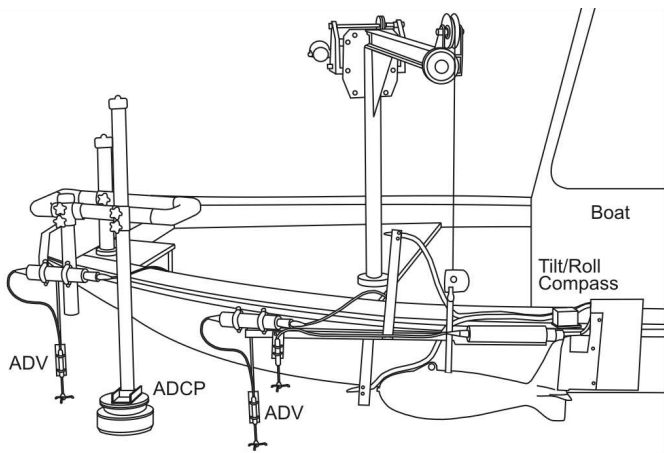
Figure 2 Experimental set-up on boat including ADCP, surface-mounted ADV, and modified P-61 with ADV's mounted

dune field where the measurements were taken. This deployment allowed the boat position to be maintained with a minimum of lateral movement. Sea anchors (large bucket(s) with holes through the bottom to allow water to pass through) were deployed from the boat stern to add stability to the anchored position.

From 15 to 20 verticals of detailed velocity measurements were collected for each of the experiments. This spatial density of observation verticals was the maximum possible given the time constraints for data collection (data collection began at dawn and terminated at dark). The verticals were located such that spacing was minimized at the crest and lee of a bedform. Discharges over the course of the data collection varied by less than 3% for the MO-1 data set and less than 1% for the MO-2 data set.

For dataset MO-1 collected on June 19, 2002, a downward-looking ADCP, mounted on the bow, measured point velocities at numerous 0.25 m bins from near the water surface to near the channel bed. As approximately 6% of the flow depth near the bed is not measurable by the ADCP, the modified P-61 was lowered to the bed and two P-61 mounted ADVs measured the velocity at locations 0.057 m and 0.42 m above the bed. For each vertical of MO-1, velocity data were collected for a total of 10 minutes. An ADV mounted on the boat enabled collection of near-surface water velocities.

After analysis of the MO-1 data, a decision was made to collect additional ADV data throughout the vertical for the MO-2 data collection test on August 27, 2002, and not only at two points near the bed and one point near the surface. This new data-collection scheme required positioning the ADV mounted on the modified P-61 at various locations in the water column, as opposed to simply resting the P-61 on the bed as in the MO-1 dataset.

The desire to position the ADV throughout the water column required a reduction in drag on the data-collection apparatus. Thus, no pump-sampler hoses were attached to the sampler and one ADV was removed from the sampler for the MO-2 data-collection effort. The original P-61 sampling capacity was to be utilized to collect any needed sediment samples. For the MO-2 test, the boat-mounted ADCP continued to be utilized to collect velocity data from just below the water surface to near the bed. The single ADV mounted on the sampler was positioned at

increments of 0.1 m for the first meter of elevation above the bed, and then successively positioned at 1 m higher increments from that point to the water surface, with the uppermost data point being just below the water surface. For each point location of the ADV, velocity data were collected for approximately 2 minutes. The ADCP data were collected during the entire time the boat was positioned at each vertical (approximately 30 minutes).

At the outset of this research, suspended-sediment data were to be collected to characterize the sediment concentration distribution. Because of the combination of equipment failure and time logistics, however, it was realized that few sediment data would be collected for these experiments. For the MO-1 data, suspended-sediment samples were collected 0.689 m above the bed for each vertical. As described earlier, the pump-sampler intakes were eliminated for the MO-2 test, with the intention that the sediment samples would be collected by using the built-in sampling capabilities of the P-61. Unfortunately, no sediment concentration data were collected for MO-2 as the P-61 solenoid mechanism malfunctioned, preventing sample collection.

5 Experimental results

5.1 Bedforms

Much research has been done in the past on the mechanics and prediction of bedforms. The physical processes underlying bedform mechanics is complex. Karim (1999) lists among the factors leading to this complexity: (1) Large number of governing variables and their interaction; (2) 3-dimensional nature of bedforms and their development; (3) Lags in the development of bedform adjustment in response to changes in the flow structure; and (4) Difficulties in measuring bedform dimensions in the field. For purposes of this study, the bedforms were categorized into two groups: (1) those approximating equilibrium dunes, and (2) those that do not approximate equilibrium dunes, such as washed-out dunes (residual waves), developing dunes, or bars.

From compiling the physical attributes of dunes from a number of sources (Yalin, 1964; Simons *et al.*, 1965; Graf, 1971; ASCE, 1966; Vanoni, 1975; van Rijn, 1984; Garcia, 1999), the following characteristics define an approximate equilibrium dune:

(1) Non-symmetric appearance ($L_S/L_L > 1$) where L_S is the length of the stoss side of the bedform and L_L is the length of the lee side of the bedform,
(2) Gradual stoss slopes (θ_S) leading up to a crest that abruptly changes to a sharper lee slope (θ_L), and
(3) Height (H_d) and wavelength (λ) of the bedform scale with flow depth (H)($H_d \sim 1/6H$; $\lambda \sim 2\pi H$).

The characteristics of the flow and bedforms encountered in the two experiments of this study are listed in Table 1. The MO-1 bedforms have geometric ratios that may indicate that they are equilibrium dunes. However, the bedforms are too symmetric ($L_S/L_L = 1.09$) to be equilibrium dunes. These bedforms likely are developing dunes, as bedforms typically become elongated and less symmetric for large flow depths, as shown in both

Table 1 General data for experiments MO-1 and MO-2

Date	MO-1	MO-2	
	June 19, 2002	August 27, 2002	
Discharge (Q)	3,160 m³/s	1,407 m³/s	
Slope (S)	0.00016	0.00017	
Mean depth ($\langle H \rangle$)	6.46 m	4.87 m	
Mean velocity (U)	1.52 m/s	1.03 m/s	
Froude number (F)	0.2	0.149	
Median bed material size (D_{50})	0.31 mm	0.31 mm	
		Large bedform	Small bedform
Dune height (H_d)	1.25 m	1.1 m	0.32 m
Dune length (λ)	23.0 m	140 m	5.7 m
Stoss angle (θ_S)	5.7°	0.72°	3.4°
Lee angle (θ_L)	7.8°	1.3°	14°–30°
Ratio of stoss to Lee length (L_S/L_L)	1.09	1.90	1.5
Near-bed total suspended sediment concentration (mg/l)		482	320
Near-bed sand suspended Sediment concentration (mg/l)		265	265

numerical perturbation analysis (Kennedy, 1963; Fredsoe, 1982) and through field observations (Shen *et al.*, 1978; Jordan, 1965).

The MO-2 bedforms are a combination of large non-symmetric bedforms with smaller superimposed, non-symmetric bedforms. The larger bedform geometries approximate those of equilibrium dune characteristics reasonably well. The geometries from all the Smith and McLean (1977) bedforms are within expected ratios that would characterize them as equilibrium dunes. The June 21, 1989 dataset from Kostaschuk and Villard (1996) had bedforms with geometries suggesting that they are non-equilibrium dunes, with the remaining 2 Kostaschuk and Villard (1996) datasets characterized as equilibrium dunes.

5.2 Mean flow

The velocity and bed profiles are shown for the datasets MO-1 and MO-2 in Figs 3 and 4. The channel bathymetries for these experiments were collected at the same resolution, but have great differences in their geometries. In both these experiments, flow separation in the lee of the bedform was detectable. MO-1 had zero near-bed velocities measured at $x = 36.3$ m and 37.6 m (3.8 m and 5.1 m downstream of the bedform crest at $x = 32.5$ m). MO-2 had negative near-bed velocities at $x = 138.9$ m (5.4 m downstream of the crest at $x = 133.5$ m). According to Nelson *et al.* (1993), the distance between the crest and the downstream reattachment point averaged about $4H_d$, which corroborates the findings of Engel (1981). Lyn (1993) discussed the re-circulation region downstream of the bedform crest and noted that in his laboratory results, the re-circulation region extended past the one-quarter length of the next downstream bedform. The spatial resolution of the MO-1 and MO-2 experiments was insufficient to definitively ascertain the reattachment point, but flow attachment was evident by location $x = 38.3$ m in MO-1, in that the near-bottom velocity had increased considerably from the
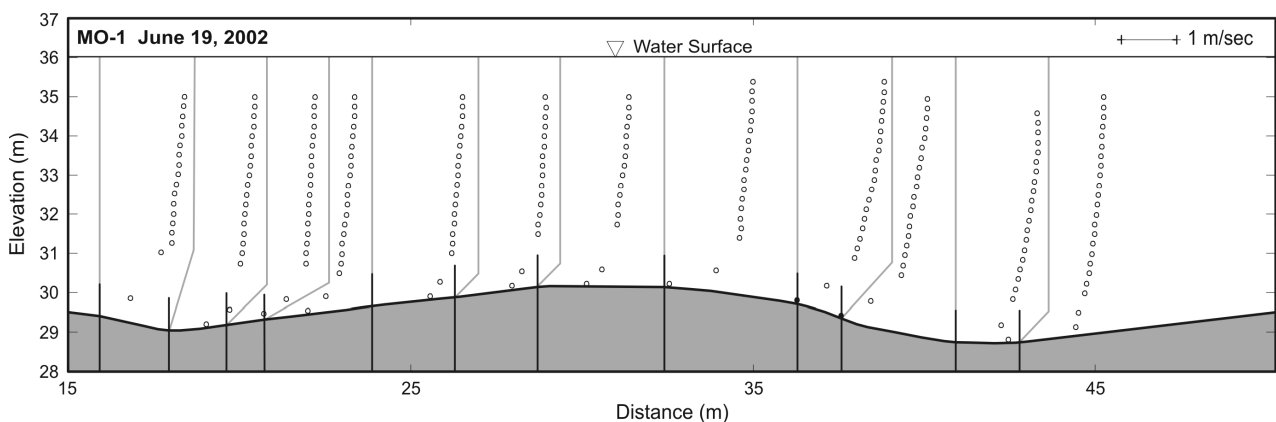

Figure 3 Streamwise velocity observations for the MO-1 data set. Vertical lines along the bottom of the plot indicate the location of the velocity profile origin. Because of data density, lighter solid lines are included to assist the reader in determining which origin corresponds with a profile
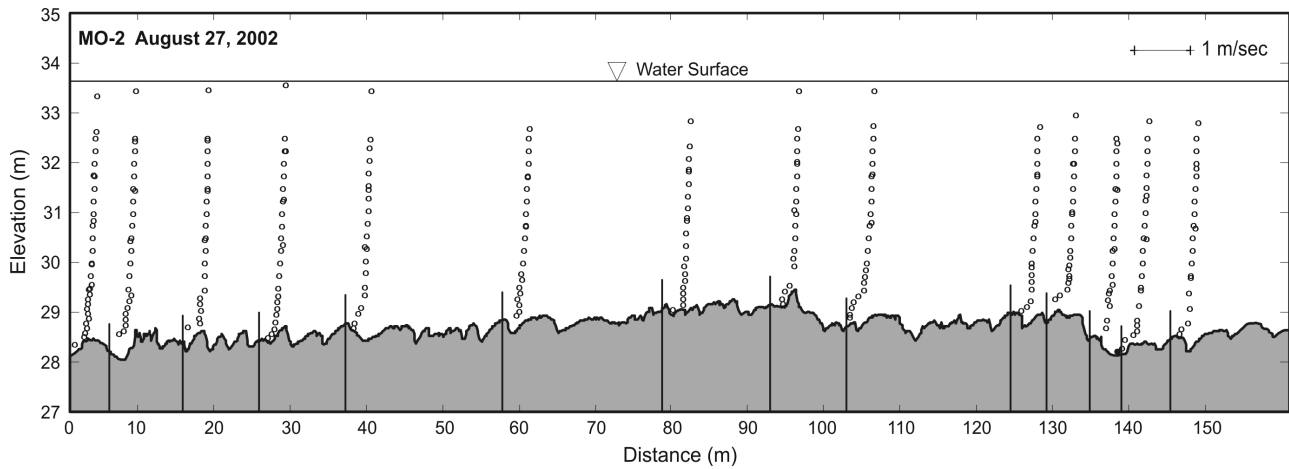
Figure 4   Streamwise velocity observations for MO-2 data set. Vertical lines along the bottom of the plot indicate the location of the velocity profile origin. Zero or negative velocities are represented as solid circles
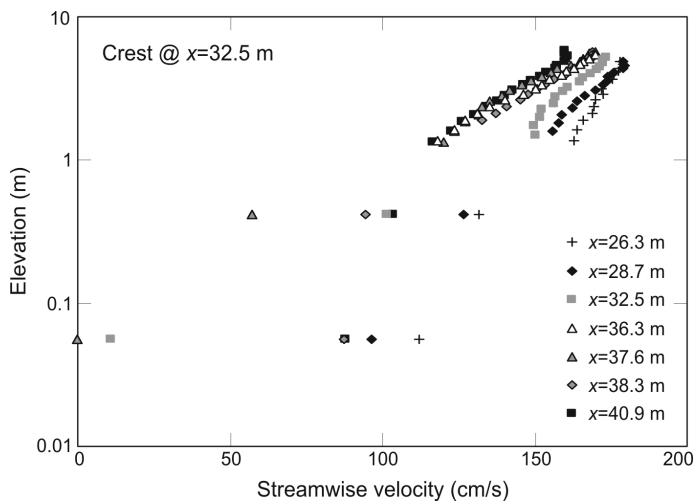

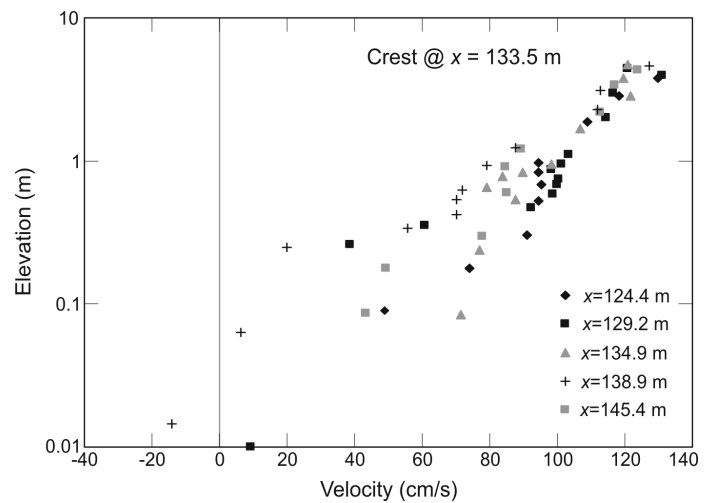Figure 5   MO-1 velocity profiles in the vicinity of the crest and in the lee of the crest

Figure 6   MO-2 velocity profiles in the vicinity of the crest and in the lee of the crest

zero velocity at $x = 37.6$ m. The attached velocity profile at $x = 38.3$ m is $4.6 H_d$ downstream of the crest. Because of the presence of the superimposed dunes in MO-2, the detailed velocity data (Fig. 4) appear to indicate the flow detaching and reattaching at numerous points along the larger parent bedform.

The attachment of the flow becomes more evident when examining the velocity profiles. Figure 5 shows a marked decrease in velocity throughout the water column downstream of the bedform crest for MO-1, which also is slightly apparent for the MO-2 experiment (Fig. 6). The question is whether the velocity decrease in MO-1 and MO-2 is a wake-induced momentum defect controlled by turbulence diffusion, or a topographically induced deceleration controlled by the pressure gradient and inertial forces. Nelson and Smith (1989) delineate the various regions of flow over well-developed bedforms as characterized by different turbulence structures and length scales. The first region is that wherein velocity and velocity fluctuations are wake-like (in the lee of the bedform near the bed and diffusing outward). A second region is present where the scaling parameters and velocity structure coincide with that of a boundary layer flow. A third region is wave-like, where the scaling parameters are

closer to those of the bulk flow parameters of shear velocity and flow depth. In MO-1 (Fig. 5), it is noted that the velocity decrease is almost immediately throughout the water column 3.8 m downstream of the crest at $x = 36.3$ m. Flow separation was noted in the MO-1 data, which would require the presence of wake-like flow features. However, the decrease of the velocity extending to the surface immediately (3.8 m) downstream of the crest likely indicates that this is attributable to the topographically induced pressure gradient, as intuitively, a wake-induced velocity decrease would require a longer distance downstream from the crest to be seen at the surface. Nelson *et al.* (1993) noted this same wave-like response of the flow to the bedforms in their laboratory experiments.

Typically, velocity scales with shear velocity, whereas the length scaling variable for the inner region is either a roughness length or a combination of the shear velocity and viscosity, where the inner region is that region where the flow is influenced by the boundary. For the outer region, that region where the influence of the boundary on the flow is decreased, the length scaling is typically the total depth. These scales typically are referred to as inner and outer scales, respectively. For the shear velocity, both

local and bulk (reach-averaged) shear velocity possibly could be used in scaling. Two common methods used to compute the bulk shear velocity u_{*T} are: (1) Square root of the product of the mean flow depth, water-surface slope, and the gravitational constant; and (2) Slope of the best-fit line through the reachwise spatially averaged velocity profile. Herein, method (1) was used to determine the bulk shear velocity, unless otherwise noted. The local shear velocity u_{*L} is computed at each vertical from the slope of the velocity distribution. In computing the local shear velocity, the velocity data in the range $0.2 < z/H < 0.5$ were typically used as this range was found to provide the most reasonable values (reasonableness was judged as smooth transition in local shear velocity along the longitudinal direction). MO-1 and MO-2 indicate a collapse of the data away from the bed to a universal functional form when scaled with shear velocity as shown in Figs 7 and 8, with the better collapse resulting with the use of the local shear velocity.

With the apparent flow separation in both the MO-1 and MO-2 data, the lack of flow similarity near the bed is to be expected. The lack of the near-bed ($z/H < 0.15$) universal flow structure
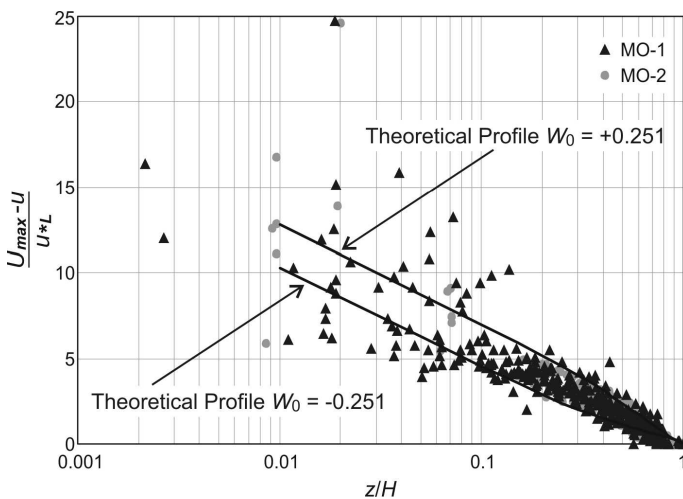

Figure 7   All local velocity data collected in MO-1 and MO-2, plotted in velocity-defect form and scaled by the local shear velocity
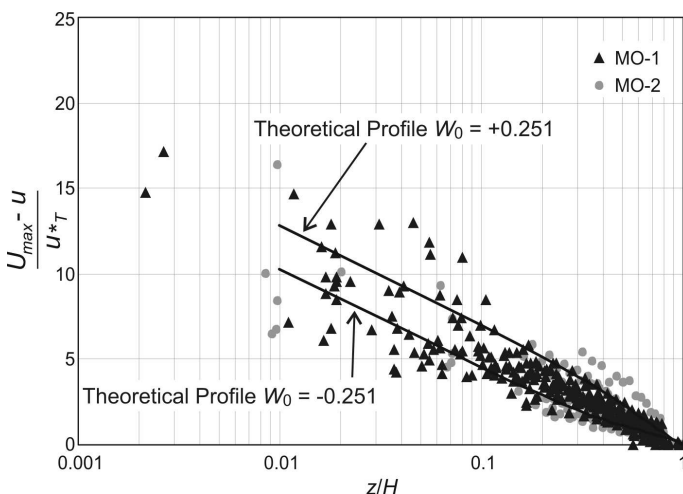

Figure 8   All local velocity data collected in MO-1 and MO-2, plotted in velocity-defect form and scaled by the bulk shear velocity

also was discussed by Lyn (1993), who noted that this region would "exhibit only weakly (if at all) universal structure." On the basis of laboratory data, Fedele and Garcia (2001) postulate that within the internal layer (near-bed region), the lack of scaling occurs as "two major dynamic mechanisms are competing in producing and transporting turbulent properties with different relative importance at different locations along flow development (shear layer and wake diffusion, and wall turbulence)". This lack of scaling seems reasonable when examining the turbulent fluctuations from the MO-2 dataset (Fig. 9). The streamwise turbulent fluctuations are similar to the wall-bounded shear flow relations given by Nezu and Nakagawa (1993) only for elevations where $z/H > 0.4$.

The velocity-defect law with a wake function can be written as

$$\frac{U_m - u}{u_*} = -\frac{1}{\kappa} \ln\left(\frac{z}{H}\right) + \frac{2W_0}{\kappa} \cos^2\left(\frac{\pi z}{2H}\right) \qquad (4)$$

where $(2W_0/\kappa) \cdot \cos^2(\pi z/2H)$ is the wake function, W_0 is Coles' wake parameter, and U_m is the maximum streamwise velocity in the water column. In this work, W_0 was computed by the method listed in Julien (1995). The rationale for this method is based on the assumption that the wake term vanishes as z approaches 0. If a semi-log plot is fitted to the lower part of the velocity profile and a line is projected to $z/H = 1$, W_0 can be calculated as

$$W_0 = \frac{\kappa}{2}\left[\frac{U_m - u}{u_*}\right]_{\frac{z}{H}=1} \qquad (5)$$

W_0 depends on free stream pressure gradients in equilibrium boundary layer flow (Lyn, 1993), with negative W_0 occurring for favorable pressure gradients and positive W_0 for adverse pressure gradients. For flat-bed flows, W_0 has a range from 0 to 0.25 with a mean of approximately 0.2 (Nezu and Rodi, 1986).

For MO-1, W_0 varied from 0.200 near the crest to -0.127 downstream of the crest (Fig. 10), with an average value for all locations of 0.020. For MO-2, W_0 varied from 0.252 at a crest of a superimposed dune to -0.251 in the lee of a superimposed bedform (Fig. 10) (Holmes, 2003). An average W_0 of 0.070 was calculated for all MO-2 locations. The impact of the range of W_0 on the theoretical velocity defect profile is shown in Figs 7 and 8.
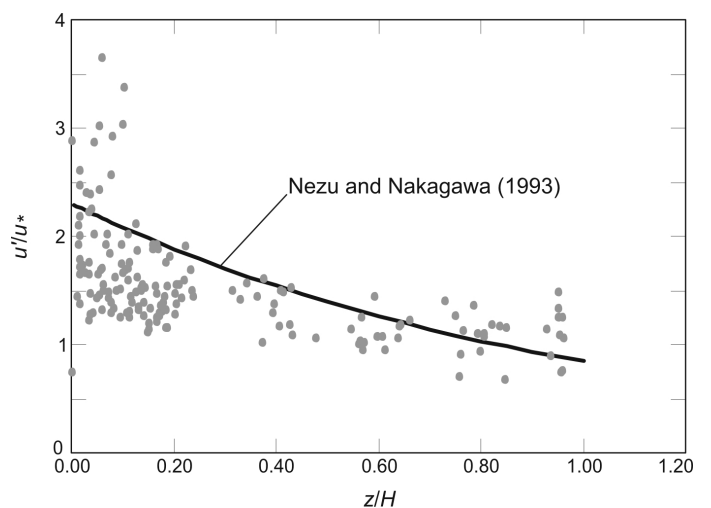

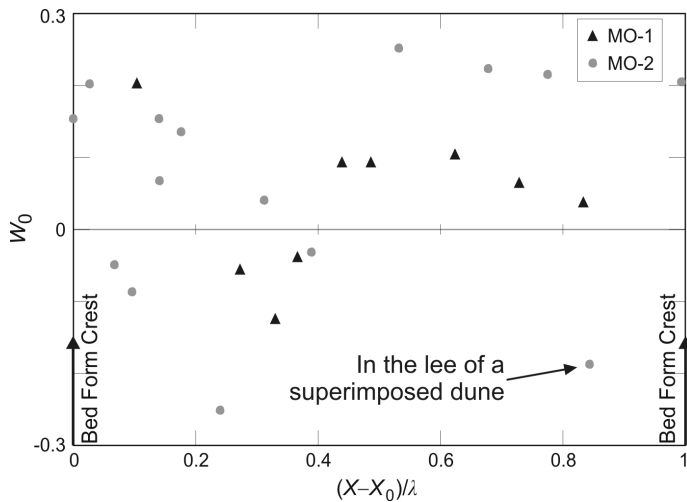Figure 9   Streamwise turbulent fluctuations for MO-2

Figure 10   Variation of Coles' wake coefficient with distance along the dune for all experiments

In general, the wake coefficient is positive in the flow leading up to the bedform crest and negative in the lee of the bedform crest (Fig. 10). The single data value that has a negative W_0 on the stoss side of the bedform, $(X - X_0)/\lambda = 0.84$, occurs in the lee of a superimposed bedform.

5.3   Spatially-averaged velocity

As shown in the above Mean Flow section, the velocity profile varies over the length of a bedform. For some applications, it is useful to determine a spatially-averaged velocity profile. These spatial averages are an integration of all the flow effects over the bedform. Various investigators performed spatial averaging of both velocity and Reynolds stresses (Smith and McLean, 1977; Nelson *et al.*, 1993; Fedele and Garcia, 2001), using two different methods: (1) Averaging along lines of constant elevation above a specified datum, and (2) Averaging along lines equidistant from the boundary, the latter being used herein. The equidistant method was judged to better capture the boundary effects in the flow structure because averaging along lines of constant elevation above the datum causes elimination of data in the bedform trough, as there are not enough other data at that elevation to average against.

For flow over bedforms, the inner length scale is the composite roughness height, k_c, which is an amalgam of both grain and form resistance. The value of k_c can be computed from the spatially averaged velocity profile. The value of C from Eq. (3) is defined as (Schlichting, 1979)

$$C = -\frac{u_*}{\kappa} \ln k_c + B\left[\frac{u_* k_c}{\nu}\right] u_* \qquad (6)$$

where $B[u_* k_c/\nu]$ is the roughness function from Nikuradse's data (Schlichting, 1979) and $u_* k_c/\nu$ is the roughness Reynolds number. Rearranging terms yields an implicit equation for k_c as

$$k_c = \exp\left\{\left(B\left[\frac{u_* k_c}{\nu}\right] - \frac{C}{u_*}\right)\kappa\right\} \qquad (7)$$

C is computed from a regression of the velocity and the natural logarithm of the elevation (z) of the velocity data point, where the intercept (for $z = 1$) of the regression fit to the line is equal

to C. The implicit nature of Eq. (7) requires an iteration process by assuming an initial value of roughness k_c, solving for the roughness Reynolds number, determining $B[u_* k_c/\nu]$ from Nikuradse's data plot (Schlichting, 1979), computing k_c by Eq. (7), and finally comparing the computed value of k_c with the initial assumption.

In examining the values for k_c, a value 0.322 m was computed for the MO-2 data set which scales with the superimposed bedform heights, whereas a computed $k_c = 0.13$ m for MO-1 is much smaller than the bedform height (Table 1). This result seems to imply that the flow for MO-1 was experiencing a smaller amount of form resistance, with the bedforms appearing to the flow as large roughness elements. The lack of form resistance is likely due to the relatively symmetric and closely spaced bedforms of MO-1.

Examining the data to determine similarity characteristics, the data can be plotted in logarithmic form with the composite roughness height as the length scaling parameter and the bulk-shear velocity as the velocity-scaling parameter. This log-linear form is presented in Fig. 11 and shows some collapse of the data toward a universal functional form. The MO-2 data seem to have two linear segments, whereas the MO-1 data could be well characterized by one single linear segment. MO-1 data were for bedforms that were not characterized as equilibrium dunes, as was the June 21 dataset collected by Kostaschuk and Villard (1996). This dataset also was represented well by a single linear segment (Holmes, 2003). MO-2, which required 2 segments to properly characterize the velocity profile in log-linear space, had equilibrium dunes present. This result is similar to datasets from the field experiments of Smith and McLean (1977) and Kostaschuk and Villard (1996). These data also required multiple linear segments to properly characterize the spatial velocity profile (Holmes, 2003).

The velocity data also can be presented in dimensionless velocity defect form using outer scales of average flow depth and bulk-shear velocity (Fig. 12), which provide a better data collapse. It should be noted that the velocity defect form requires no knowledge of equivalent composite roughness. The data collapse in proximity of the bed is noticeably improved as compared to the local velocity data (Figs 7 and 8).
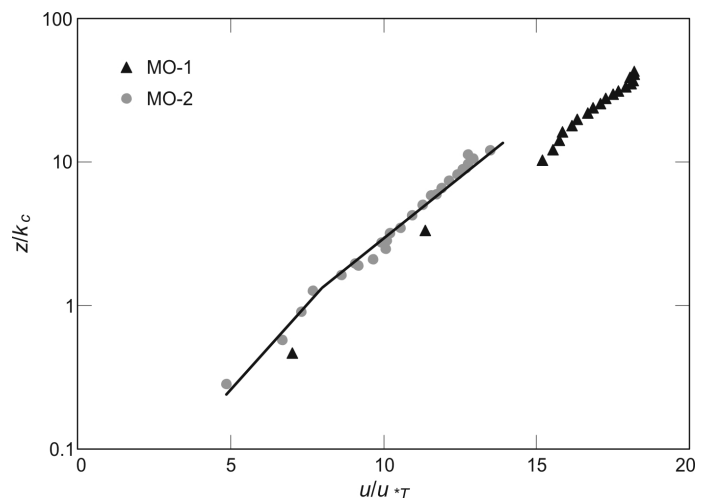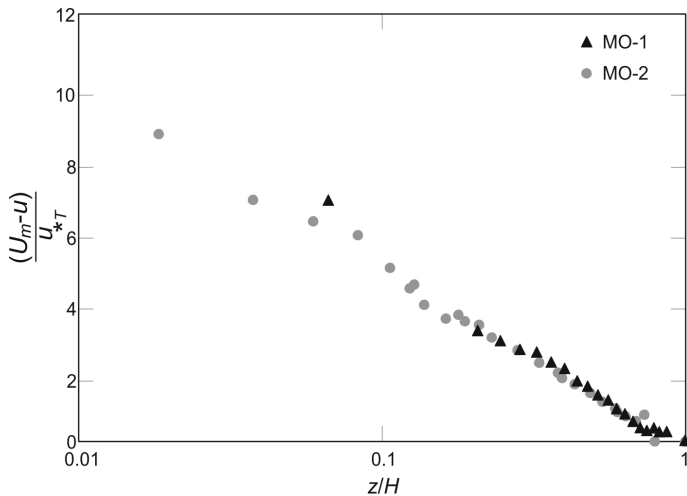

Figure 11   Log-linear dimensionless velocity plot

Figure 12   Spatially-averaged velocity data plotted in velocity-defect form

Figure 13   Coles' wake parameter as a function of the gross flow Richardson number

6   Spatially-averaged velocity-defect model

To provide a simple model for field application, the defect form of the log-linear velocity model Eq. (4) can be used without knowledge of the roughness parameters k_s or k_c. The parameters to be estimated for application of the velocity-defect model are U_m, u_*, (either u_{*T} or u_{*L}) and W_0. The inclusion of the wake adds non-linearity (in log-linear space) to the velocity profile. The wake function accounts for some of the pressure and inertial effects that are not accounted for in the log-law velocity models. A number of measures of bedform geometry were investigated to determine if they were uniquely related to W_0; however, nothing satisfactory was found. Coleman (1986) determined that W_0 varies with sediment concentration, which is in-line with other work suggesting the influence of sediment on the velocity profile (Vanoni, 1946; Einstein and Chien, 1955; Coleman, 1981; Gelfenbaum and Smith, 1986). Given those findings, an effort was made to determine a relation between W_0 and the sediment concentration. As the sediment concentration can be expressed in terms of the gross flow Richardson number, R_{ig}, a relation between R_{ig} and W_0 was developed (Fig. 13) based on (Coleman, 1986)

$$\mathsf{R}_{ig} = \frac{gH(\rho_s - \rho_f)}{\langle \rho_f \rangle U_m^2} \tag{8}$$

where $\langle \rho_f \rangle$ is the vertically-averaged sediment-water mixture density, U_m is the maximum water velocity, H is the average flow depth, and ρ_s is sediment density. For this work, ρ_f is defined as the sediment-water mixture density near the bed (approximately 0.005 m above the bed). This simpler version for computation of R_{ig} in Eq. (8) was used because of the limited sediment concentration data.

Three field datasets [69-W1 of Smith and McLean (1977), June 29 of Kostaschuk and Villard (1996), and MO-2] were not used in Fig. 13, so that these data could be used to test the velocity-defect profiles predicted with the W_0 estimated from Fig. 13.

The sediment concentration distribution used to compute the vertical average of the sediment-water mixture density $\langle \rho_f \rangle$ was determined by applying the sediment distribution of Rouse to
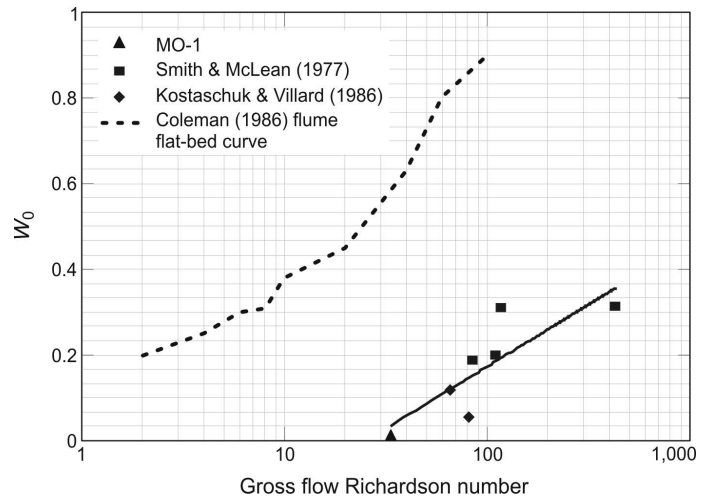
the near-bed suspended-sediment sample. The MO-2 suspended-sediment concentration near the bed was estimated from a combination of the MO-1 data and the detailed suspended-sediment data collected 112 km upstream at the Missouri River at Hermann, Mo. The flow conditions and bed-sediment sizes are there similar to those at St. Charles. Sand and total suspended-sediment concentrations near the bed are listed in Table 1. The density at each location in the vertical was then computed as

$$\rho_f = \rho_s c + \rho(1 - c) \tag{9}$$

where c is the volumetric sediment concentration.

The relation between the Richardson number and Coles' wake parameter from the original laboratory flume work of Coleman (1986), using flat beds, is also shown in Fig. 13. As Coles' wake parameter is used to help account for pressure and inertial forces, a difference in the relation between flows over bedforms and the flat-bed flows is to be expected. For field applications, a log-linear relation fit through the data can be used to estimate Coles' wake parameter, the bulk shear velocity can be computed from

$$u_{*T} = u_* = \sqrt{g\langle H \rangle S} \tag{10}$$

and the maximum velocity and total depth are fairly easy to determine. From these parameters, the velocity profile can be computed from Eq. (4). Plots of the model performance in comparison to the field observed data of MO-2 are shown in Fig. 14. A summary plot of velocity-defect model performance for the validation datasets of MO-2, Smith and McLean 69-W1 (1977), and Kostaschuk and Villard June 29 (1996) is shown in Fig. 15. The velocity-defect model is accurate away from the bed ($z/H > 0.1$), where the error is ±10% in all cases, whereas the accuracy is eroded considerably near the bed ($z/H < 0.1$). This accuracy decrease is especially true for those situations in which the bed becomes more dune-like with increasing lee vortices and the flow separation is strong resulting in a definitive two-segment, log-linear velocity profile, such as for the Smith and McLean (1977) 69-W1 dataset. The vertically-averaged mean velocities for modeled velocity profiles for the three verification datasets in Fig. 15 had an averaged absolute error of 2.7% for the three data
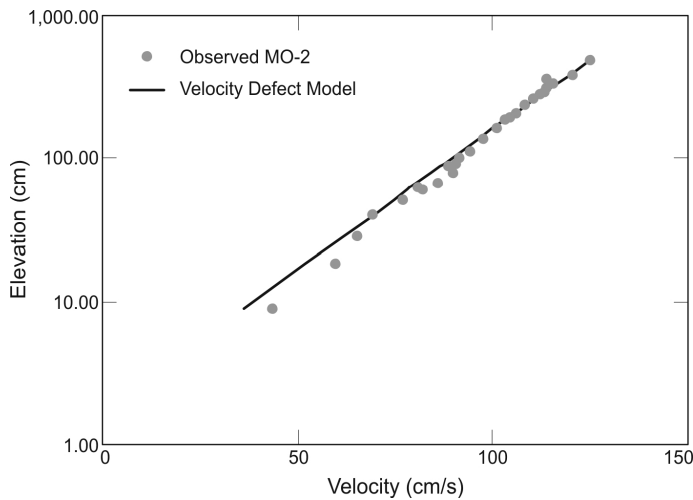
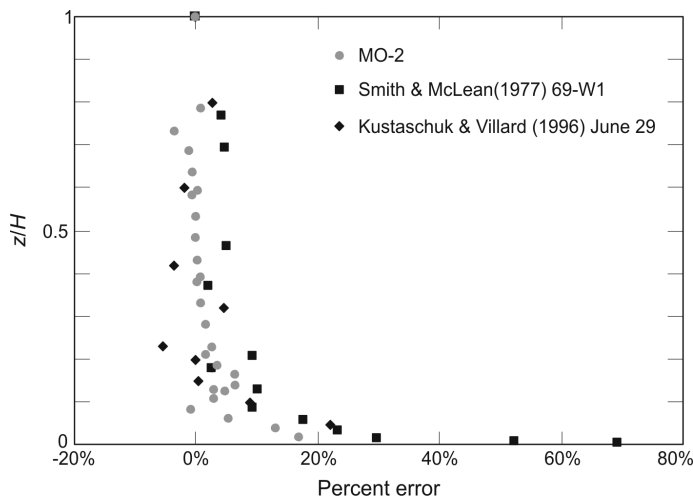Figure 14   Observed and velocity-defect modeled velocity profiles for MO-2 data

Figure 15   Error of the velocity-defect model as a function of dimensionless elevation above the bed

Figure 16   Error of the velocity-defect model, neglecting W_0, as a function of dimensionless elevation above the bed

sets with all modeled velocity profiles within 5% of the observed mean velocity.

The weakness of the spatially-averaged W_0 is recognized, particularly when one evaluates it in light of the variation of W_0 over a bedform (Fig. 10). As such, the performance of the velocity defect model without considering W_0 was also evaluated. Figure 16 shows a summary plot of velocity-defect model performance for the same validation datasets used in Fig. 15. In comparison to the velocity-defect model with W_0, the velocity-defect model without W_0 has little, if any, decrease in performance away from the bed ($z/H > 0.3$), where the error is $\pm 10\%$ in all cases and has model accuracy decreases in the range $z/H < 0.1$. In this near-bed range, the errors greatly increase. However, the modeled vertically-averaged mean velocities for the velocity-defect model without W_0 has a much lower average absolute error value of 0.4%, with all modeled vertically-averaged mean velocities within 0.8% of the observed vertically averaged mean velocities. In addition, the model has the added advantage of easier field application, as there is no need for knowledge of the sediment concentration.
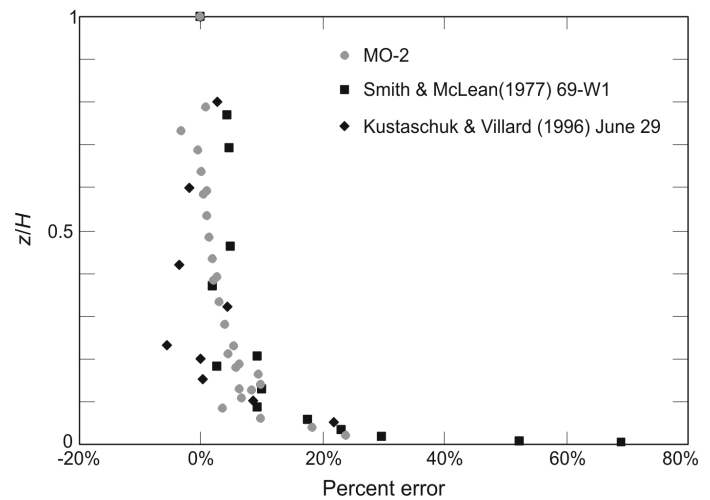
7   Conclusions

A field study of flows over bedforms, utilizing ADCP and ADV instrumentation, was conducted on the Missouri River at St. Charles, Mo. The MO-2 dataset was determined to have bedforms that approximated equilibrium dunes with superimposed dunes, whereas equilibrium dunes were not present in the MO-1 dataset. The spatially-averaged and at-a-vertical velocity distributions were logarithmic in nature for all datasets. Flow separation in the lee of the bedforms was noted in both datasets, with the smaller superimposed bedforms appearing to be the controlling feature on the MO-2 data. There is good collapse to a universal functional form of the spatially-averaged field-scale velocity data in both inner and outer scales (log-linear and velocity-defect form). Coles' wake coefficient, computed for all velocity profiles at each section, varied from 0.200 near the crest to -0.127 downstream of the crest for the MO-1 dataset, and from 0.252 at a crest of a superimposed dune to -0.251 in the lee of a superimposed bedform for the MO-2 dataset. The flow over the bedforms experiences a wave-like response in the outer region, with velocity decreasing throughout the flow depth over bedform troughs, and the velocity increasing over bedform crests.

The spatially averaged velocity profiles for those experiments with bedforms that do not approximate equilibrium bedforms can be well characterized with a single logarithmic function, whereas flows over equilibrium dunes require multiple linear segments in logarithmic space to characterize the profile. All the field data collected in this research collapse sufficiently well when plotted in inner scales (bulk-shear velocity and the composite roughness length); the collapse is better, however, when the data are plotted in velocity-defect form. There appears to be universal flow structure close to the bed in the spatially averaged data.

The standard velocity-defect-wake model was tested for the spatially averaged velocity profiles of field data, with bedforms present. Coles' wake parameter was presented as a function of the gross flow Richardson number, which requires some knowledge of the vertical-density distribution where sediment concentration influences the density. The model estimates the

vertically-averaged mean velocity to within 2% and estimates the point velocities to within $\pm 10\%$ for $z/H > 0.1$. The velocity-defect model without the Coles' wake parameter was evaluated and found to estimate the vertically-averaged mean velocity better than the velocity-defect model that included Coles' wake parameter.

Acknowledgments

Notation

$B[u_* k_c/\nu] =$ Roughness function
$c =$ Volumetric sediment concentration
$C =$ Constant
$D_{50} =$ Median diameter of bed material
$\mathsf{F} = u/(gH)^{1/2}$ Froude number
$g =$ Acceleration of gravity
$H =$ Flow depth
$\langle H \rangle =$ Spatially-averaged flow depth
$H_d =$ Bedform height
$k_c =$ Composite roughness height
$k_s =$ Nikuradse equivalent roughness parameter
$L_s =$ Length of stoss side of bedform
$L_L =$ Length of lee side of bedform
$p =$ Pressure
$Q =$ Streamflow discharge
$\mathsf{R}_{ig} =$ Gross Richardson number
$S =$ Water surface slope
$u =$ Mean velocity at a point
$U =$ Vertically-averaged mean velocity
$U_m =$ Maximum streamwise velocity in water column
$u_* =$ Shear velocity
$u_{*L} =$ Local shear velocity
$u_{*T} =$ Bulk (reach-averaged) shear velocity
$u_* k_c/\nu =$ Roughness Reynolds number
$W_0 =$ Coles' wake coefficient
$x =$ Distance along bedform; streamwise coordinate
$x_0 =$ Location of the bedform crest

Greek symbols

$z =$ Elevation above channel bed, vertical coordinate
$\kappa =$ Von Karman's constant
$\lambda =$ Bedform length
$\mu =$ Dynamic viscosity
$\theta_s =$ Stoss side angle of bed form
$\theta_L =$ Leeside angle of bed form
$\rho_f =$ Fluid density
$\langle \rho_f \rangle =$ Spatially-averaged fluid density
$\rho_s =$ Sediment density

References

ASCE Task Force on Bed Forms in Alluvial Channels of the Committee on Sedimentation. (1966). Nomenclature for bed forms in alluvial channels. *J. Hydr. Div., ASCE* 92(3), 51–64.

ASCE Task Force on Flow and Transport Over Dunes. (2002). Flow and transport over dunes. *J. Hydr. Engng.* 128(8), 726–728.

Bennett, S.J., Best, J.L. (1995). Mean flow and turbulence structure over fixed, two-dimensional dunes: Implications for sediment transport and bedform stability. *Sedimentology* 42, 491–513.

Coleman, N.L. (1981). Velocity profiles with suspended sediment. *J. Hydr. Res.* 19(3), 211–229.

Coleman, N.L. (1986). Effects of suspended sediment on the open-channel velocity distribution. *Water Resources Research* 22(10), 1377–1384.

Einstein, H.A., Chien, N. (1955). Effects of heavy sediment concentration near the bed on velocity and sediment distribution. *Report* 8. U.S. Army Corps of Engineers, Missouri River Division, University of California, Berkley, California.

Engel, P. (1981). Length of flow separation over dunes. *J. Hydr. Div., ASCE* 107(10), 1133–1143.

Fedele, J.J., Garcia, M.H. (2001). Alluvial roughness in streams with dunes: A boundary-layer approach. In *River, Coastal, and Estuarine Morphodynamics*, G. Seminara, P. Blondeaux (eds.), Springer, Berlin, pp. 37–60.

Fredsoe, J. (1982). Shape and dimensions of stationary dunes in rivers. *J. Hydr. Div., ASCE* 108(HY8), 932–947.

Garcia, M.H. (1999). Sedimentation and erosion hydraulics. In *Hydraulic Design Handbook*, L.W. Mays (ed.), McGraw-Hill, New York, pp. 6.1–6.113.

Gelfenbaum, G., Smith, J.D. (1986). Experimental evaluation of a generalized suspended-sediment transport theory. In *Shelf Sands and Sandstones*, R.J. Knight, J.R. McLean (eds.), Canadian Society of Petroleum Geologists, Calgary, pp. 133–144.

Graf, W.H. (1971). *Hydraulics of Sediment Transport*. McGraw-Hill, New York.

Helsel, D.R., Hirsch, R.M. (1992). *Statistical Methods in Water Resources*. Elsevier, Amsterdam NL.

Holmes, R.R., Jr. (2003). Vertical velocity distributions in sand-bed alluvial rivers. PhD Dissertation, University of Illinois, Urbana-Champaign.

Jordan, P.R. (1965). Fluvial sediment of the mississippi river at St. Louis, Missouri. *U.S. Geological Survey Water-Supply Paper* 1802.

Julien, P.Y. (1995). *Erosion and Sedimentation.* Cambridge University Press, Cambridge UK.

Karim, F. (1999). Bed-form geometry in sand-bed flows. *J. Hydr. Engng.* 125(12), 1253–1261.

Kennedy, J.F. (1963). The mechanics of dunes and antidunes in erodible-bed channels. *J. Fluid Mech.* 16, 521–544.

Kostaschuk, R., Villard, P. (1996). Flow and sediment transport over large subaqueous dunes: Fraser river, Canada. *Sedimentology* 43, 849–863.

Lyn, D.A. (1993). Turbulence measurements in open-channel flows over artificial bed forms. *J. Hydr. Engng.* 119(3), 306–326.

Nelson, J.M., Smith, J.D. (1989). Mechanics of flow over ripples and dunes. *J. Geophysical Res.* 94(C6), 8146–8162.

Nelson, J.M., McLean, S.R., Wolfe, S.R. (1993). Mean flow and turbulence fields over two-dimensional bed forms. *Water Resources Res.* 29, 3935–3953.

Nezu, I., Rodi, W. (1986). Open-channel flow measurements with a laser doppler anemometer. *J. Hydr. Engng.* 112(5), 335–355.

Nezu, I., Nakagawa, H. (1993). *Turbulence in Open-Channel Flows*. IAHR Monograph Series. Balkema Rotterdam NL.

Prandtl, L. (1904). Über Flüssigkeitsbewegung bei sehr kleiner Reibung. *Proc. 3rd Intl. Congress of Mathematics*, Heidelberg, pp. 484–491.

Rouse, H., Ince, S. (1963). *History of Hydraulics*. Dover, New York.

Schlichting, H. (1979). *Boundary-Layer Theory*, 7th ed. McGraw-Hill, New York.

Shen, H.W., Mellema, W.J., Harrison, A.S. (1978). Temperature and Missouri river stages near Omaha. *J. Hydr. Div., ASCE* 104(1), 1–20.

Simons, D.B., Richardson, E.V., Nordin, C.F. (1965). Sedimentary structures generated by flow in alluvial channels. *American Assoc. Petroleum Geologists, Special Publication* 12. AAPG, Tulsa, OK.

Smith, J.D., McLean, S.R. (1977). Spatially averaged flow over a wavy surface. *J. Geophysical Res.* 82(12), 1735–1746.

van Rijn, L.C. (1984). Sediment transport III: Bed forms and alluvial roughness. *J. Hydr. Engng.* 110(12), 1733–1754.

Vanoni, V.A. (1946). Transportation of suspended sediment by water. *Trans. ASCE* 111, 67–133.

Vanoni, V.A. (1975). *Sedimentation Engineering*. Manual 54. ASCE, New York.

Yalin, M.S. (1964). Geometrical properties of sand waves. *J. Hydr. Div., ASCE* 90(5), 105–120.

Yen, B.C. (1992). Hydraulic resistance in open channels. In *Channel Flow Resistance: Centennial of Manning's Formula*, B.C. Yen, (ed.), Water Resources Publications, Littleton Co., pp. 1–135.